Physica E 44 (2012) 1182–1188

Contents lists available at SciVerse ScienceDirect

Physica E

journal homepage: www.elsevier.com/locate/physe

Laser stimulated optical features of gold nanoparticles attached on ITO substrate

M.A. Aziz [a], M. Oyama [a], Ali H. Reshak [b,c], E. Gondek [d], P. Armatys [e], Ahmed Shebl [g], I.V. Kityk [f,*], A. Wojciechowski [f], W. Otowski [d]

[a] Department of Material Chemistry, Graduate School of Engineering, Kyoto University, Nishikyo-ku, Kyoto 615-8520, Japan
[b] School of Complex Systems, FFWP-South Bohemia University, Nove Hrady 37333, Czech Republic
[c] School of Material Engineering, Malaysia University of Perlis, P.O. Box 77, d/a Pejabat Pos Besar, 01007 Kangar, Perlis, Malaysia
[d] Institute of Physics, Cracow University of Technology, Podchorazych 1, 30-084 Krakow, Poland
[e] AGH - University of Science and Technology, Faculty of Physics and Applied Computer Science, al. A. Mickiewicza 30, 30-059 Krakow, Poland
[f] Electrical Engineering Department, Czestochowa University of Technology, Aleja, Armii Krajowej 17/19, PL-42-201 Czestochowa, Poland
[g] Department of Chemistry, Faculty of Science, Ain Shams University, Abbassia, Cairo, Egypt

ARTICLE INFO

Article history:
Received 1 November 2011
Received in revised form
11 January 2012
Accepted 17 January 2012
Available online 14 February 2012

ABSTRACT

We have performed complex studies of regular sized gold nanoparticles (AuNPs), which were commercially available and attached on the surfaces of indium tin oxide (ITO) substrates with a cross-linker molecule, 3-aminopropyltrimethoxysilane. Using the hyperfine AFM methods including the surface topology we have classified three types of samples which are different by the sizes. We have studied their laser induced absorption and third harmonic generation versus the sizes of nanoparticles. The particular influence of size dispersion on the output optical and nonlinear optical effects are studied. The processes are explained within a framework of interactions between the surface Plasmon resonances and the inter-band transitions.

1. Introduction

Gold nanoparticles (AuNPs) have attracted much interest for their application in biosensing due to their distinctive optical property known as surface plasmon resonance (SPR) as well as their biocompatibility [1,2]. Localized surface plasmons (LSPs) are charge density oscillations confined to metallic NPs. Excitation of LSPs by incident light results in the appearance of intense surface plasmon (SP) absorption band, which is affected by the changes in refractive index of nanoparticle proximity [3–5]. On the other hand, propagating SPs, which are charge density oscillations at a metal thin film deposited onto the surface of a dielectric, and their application in SPR sensors have been intensively studied to develop a label-free biosensor [6–8]. Gold nanoparticles can be prepared in the form of nanowires [9] or cross-linked hybrid AuNP-fullerene films [10].

Localized surface plasmon resonance (LSPR) of twin-linked gold nanoparticles deposited onto transparent indium tin oxide (ITO) has been used as a label-free optical biosensor of an enzyme goat anti-mouseimmunoglobulin G [11]. LSPR excitation was found to depend on the particle alignment, interparticle distance and excitation wavelength [12]. Hence, this structure can be detected with a small change of refractive index such as biomolecular interactions for biosensing applications.

Surface plasmon resonance of gold nanoparticles has attracted much attention in the past decade. Plasmon–plasmon interactions between the gold nanoparticles [13], optical properties of SiO_2 covered with gold [14] as well as electrochemical and spectral characteristics of AuNP-covered ITO electrode [15] have been reported.

Gold nanoparticles are known to exhibit nonlinear optical properties. For example, triangular-shaped Au/ZnO nanoparticle arrays show great potential for future optical devices. The real and imaginary parts of third-order nonlinear optical susceptibility of such system, $\mathrm{Re}\chi^{(3)}$ and $\mathrm{Im}\chi^{(3)}$, were determined to be 1.15×10^{-6} and -5.36×10^{-7} esu, respectively [16]. It has also been shown that periodic Au nanoparticle arrays exhibit a fast third-order nonlinear optical response with the nonlinear refractive index and nonlinear absorption coefficient being $n_2=6.09\times10^{-6}\,\mathrm{cm^2/kW}$ and $\beta=-1.87\times10^{-6}\,\mathrm{m/W}$, respectively [17]. Aggregated nanostructures of gold in hydrophobic poly(etherimide) membranes have demonstrated three-photon type nonlinear absorption attributed to excited state absorption occurring in the nanostructures [18]. Interestingly, the nonlinearity is more prominent in the aggregated nanostructures compared to the spherical nanostructures. These materials are potential candidates for optical limiting

* Corresponding author.
E-mail address: iwank74@gmail.com (I.V. Kityk).

1386-9477/$ - see front matter © 2012 Elsevier B.V. All rights reserved.
doi:10.1016/j.physe.2012.01.008

applications as well. In Ref. [19], AuNPs deposited on the ITO substrate have been studied. It was found that the maximal bicolor (1064 nm and 532 nm) stimulated optical second harmonic generation was observed for the samples possessing irregular Au NPs deposited on ITO.

As gold nanoparticles present an interesting and still quite unexplored class of nonlinear-optics materials, we decided to examine third harmonic generation (THG) abilities of AuNPs covalently attached to ITO-coated glass. In particular, using the commercially available regular sized AuNPs of 20, 30, 40 and 50 nm obtained from BB international, UK, it is expected that the effects of the size of AuNPs can be explored without suffering the irregularity of AuNPs as observed in the case of the seed-mediated grown AuNPs [19]. In this study we present preparation, photo-induced absorption spectra, AFM surface study and THG generation ability of the 20–50 nm AuNPs on transparent ITO electrodes.

2. Experimental

2.1. Preparation of 20, 30, 40 and 50 nm AuNPs attached on ITO

The colloidal solutions containing 20, 30, 40 and 50 nm gold nanoparticles (AuNPs) were purchased from BB International, UK. Trichloroethylene, an aqueous solution of ammonium hydroxide (30%) and 3-aminopropyltrimethoxysilane (APTMS) were obtained from Sigma-Aldrich. Ethanol and aqueous solution of hydrogen peroxide (30%) was from Wako Pure Chemicals. The indium tin oxide (ITO) coated glass was purchased from Geomatec, Japan (Table 1).

Initially, a piece of ITO was cleaned with trichloroethylene, ethanol and water successively and dried. Next, the cleaned ITO was heated at 70 °C for 1.5 h in the mixture of water, ammonium hydroxide (30%) and hydrogen peroxide (30%) (5:1:1(v/v)) and followed by washing with water. After drying, the ITO was immersed in ethanol containing 2% APTMS (v/v) overnight at room temperature to prepare APTMS-modified ITO that has amino terminals on the surface. Next, it was washed with ethanol, and subsequently dried with nitrogen blowing. Afterward, the APTMS-modified ITO was immersed in the colloid solution of 20 (or 30, 40, 50) nm AuNPs for 2 h at room temperature. The colloidal solutions were used as received. After washing with water and drying, the varied sized AuNPs attached ITO was obtained. Their size distribution is presented in Figs. 1–4.

2.2. Topology of sample surfaces

Topography and phase contrast images of the 20, 30, 40 and 50 nm AuNPs were collected in air at room temperature with atomic force microscopes Agilent 5500AFM working in non-contact mode. AFM micrographs were analyzed with Gwyddion software. For each sample the several places were examined in the scale of $5 \times 5\ \mu m^2$. We find regions with and without the grains on the substrate. The regions with grains seem to be well defined. A further analysis was done for the places lying away from the regions without grains. Phase imaging refers to the

Table 1
Surface characteristics of AuNPs attached to ITO.

Sample (nm)	Covered area (%)	Grain size (nm)	Grain height (nm)	Grains (μm^2)
20	74	44	19	320
30	49	70	36	80
40	23	80	48	20
50	20	82	51	18

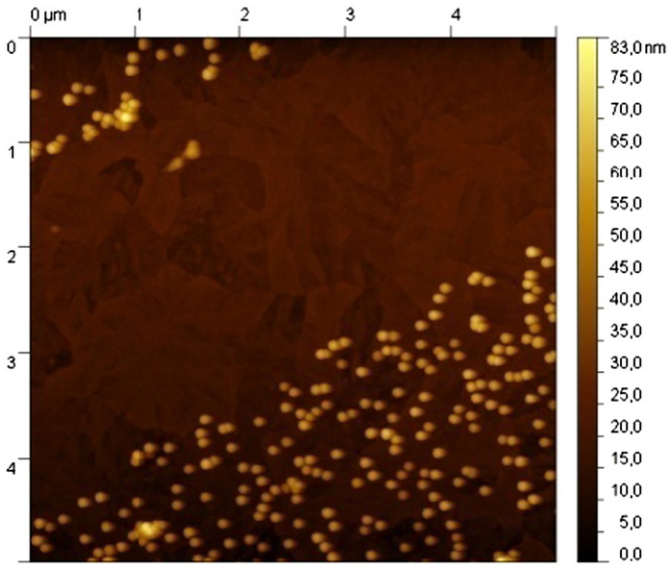

Fig. 1. Typical AFM morphology demonstrating size distribution.

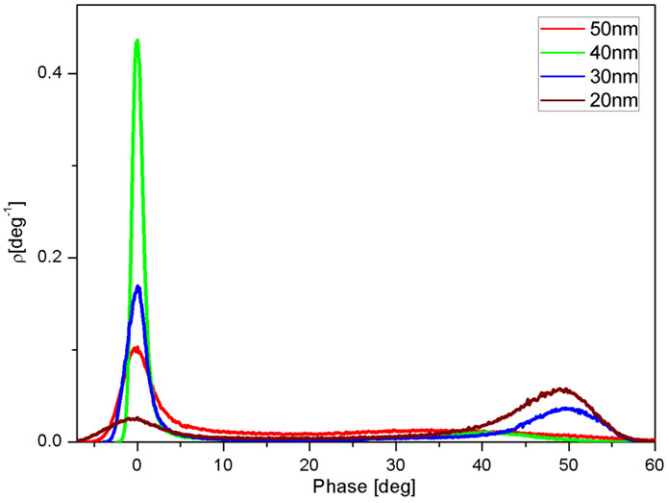

Fig. 2. Radial function angle-dependent size distribution of the nanoparticles.

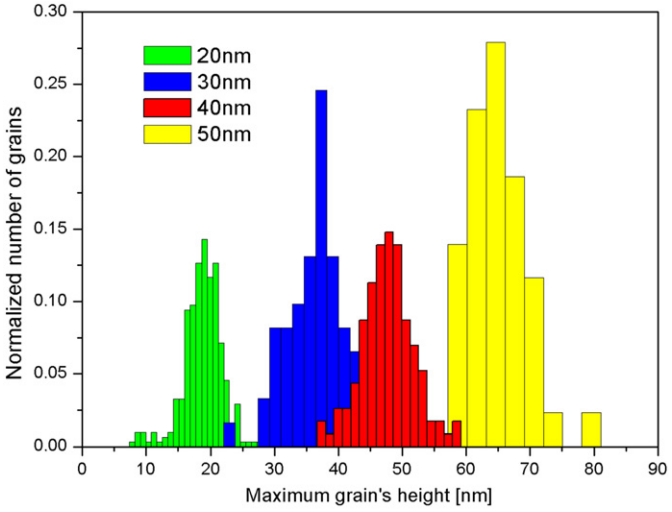

Fig. 3. Particle size distribution of 20, 30, 40, and 50 nm AuNP derived from AFM images. The size distribution is uni-modal in all the cases.

monitoring of the phase lag between the signal that drives the cantilever oscillation and the cantilever oscillation output signal. Changes in the phase lag reflect changes in the mechanical properties such as elasticity, adhesion or friction of the sample surface. The system's feedback loop operates in the usual manner, using changes in the cantilever's deflection or vibration amplitude to measure sample topography. The phase lag is monitored while the topographic image is being taken so that images of topography and material properties can be collected simultaneously.

Following the data about the morphology of the AuNP one can conclude that their sizes and shapes are highly monodispersed and the inter-particle distances are well defined. The latter is dependent on the sizes of the average AuNP. Such good structural separation of the particular nanoparticles together with their separation from the conducting ITOP substrate is a minimum criterion for their use as materials for perfect interactions with external electromagnetic light and laser coherent particularly.

3. Photoinduced optical effects

The photoinduced absorption was studied by optical fiber spectrophotometer ocean optics. This has registered the changes of transparency and related absorption under the influence of cw second harmonic Nd:YAG laser at 532 nm. The power of the laser beam was equal to about 350 mW and the beam profile was Gaussian-like. The thermoheating did not exceed 3K. The

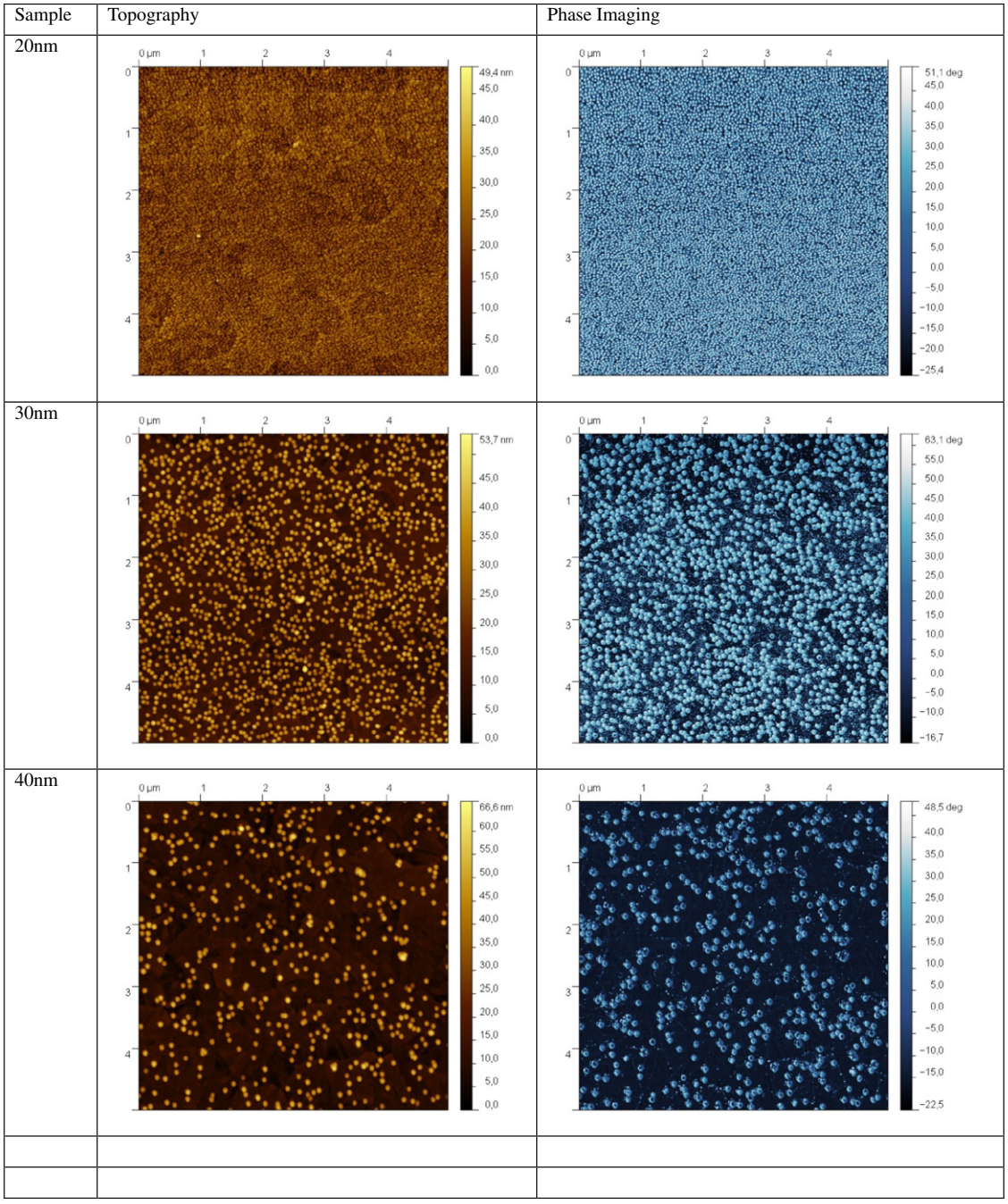

Fig. 4. The topography and phase imaging microscopy of the studied Au NP presented in different scalings.

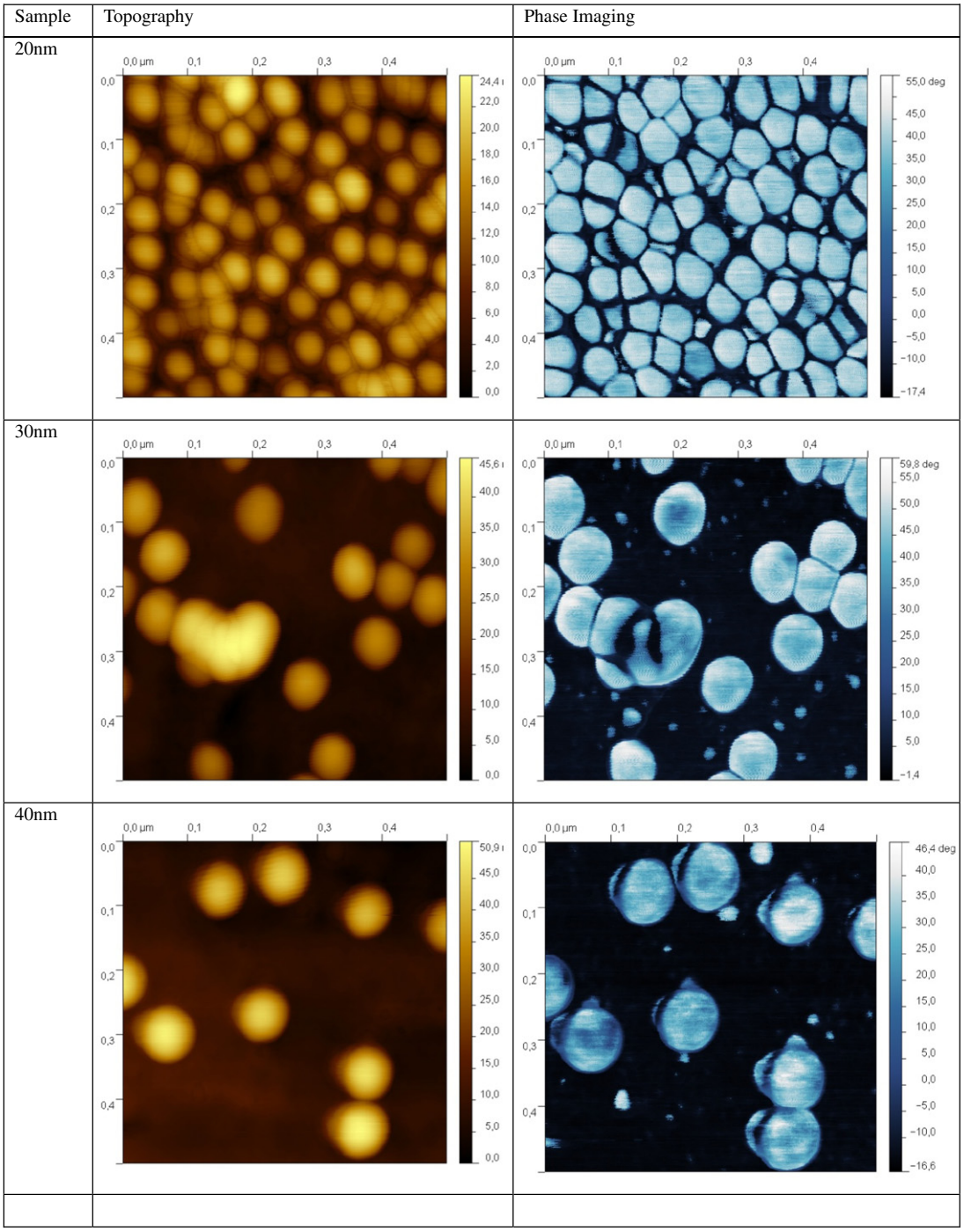

Fig. 4. (*continued*)

principal mechanisms are related to photoexcitations of the valence electrons and their trapping by the defect states and interaction with the surface plasmon excitations. The third harmonic signal from the 1064 nm Nd:YAG laser at 355 nm was registered using a filter at 355 nm and was detected by fast response photodetector using the corresponding filter. The light scattering was controlled by measurements of the reflected light within the angles 10–45° and these values were not higher than 6% with respect to the signal. The performed microsocpical observation of the surfaces did not show any signs of photodestruction.

There are three bands observed in the photo-induced absorption spectra of Au NPs/ITO situated at about 350 nm, 430 nm and 580 nm (Figs. 5 and 6). The first band at about 350 nm is attributed to the inter-band recombination of the valence d-band electrons with the holes in the conduction sp-band [20].

The second band at about 430 nm is attributed to ITO substrate defects absorption since the plasmons of Au nanoparticles could charge the empty ITO defects. This could occur at the expense of surface Plasmon resonance so it may be responsible for the weakness of the surface plasmon resonance at about 580 nm "the third band". It is crucial that the photoinduced process is continued after the interruption of the laser illumination.

From Fig. 7 one can clearly see that with decrease of the NP sizes the output THG, which is described as a third-order

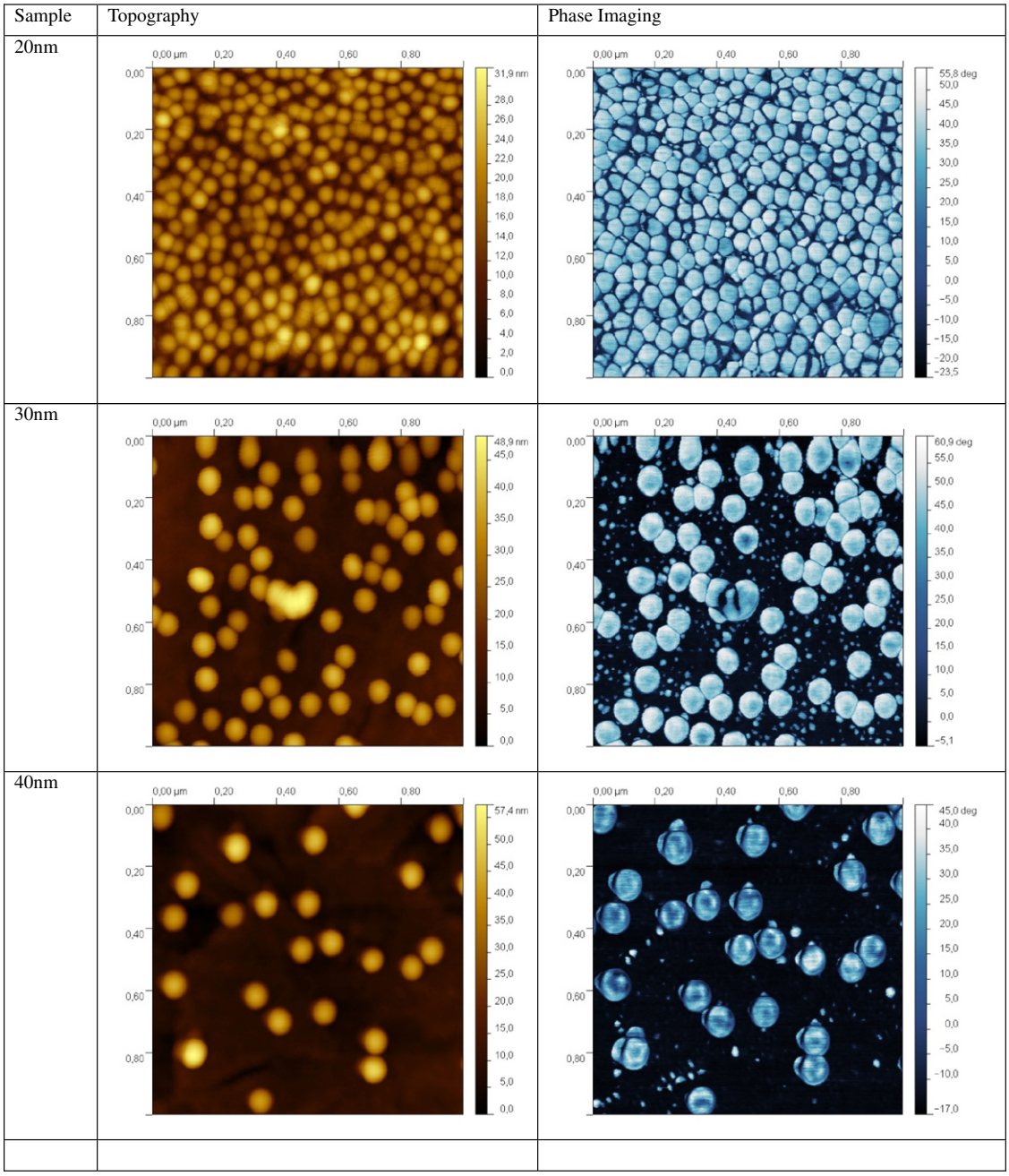

Fig. 4. (*continued*)

susceptibility, is enhanced. This enhancement is stronger at low temperatures, particularly at liquid helium temperature.

It is clear that the observed effects are caused by the photocharging of the trapping levels originated from the metallic interfaces as well due to the trapping levels located on the borders between the films and the ITO surfaces. The mentioned trapping levels effectively interact with the surface plasmon excitations. These form the electronic states which substantially change the observed photoinduced mechanisms through the changes of the ground state dipole moments. A crucial role for the photoinduced stimulated enhancement of the optical constants is also played by a good size dispersion, which in this case is virtually perfect. It is a consequence of the nano-confined effects causing an enhanced localized dielectric susceptibility. For such effects the perfect grain sizes and almost the sphere-like topology are desirable, because for the samples with the more complicated topological surfaces the THG effects are smaller. The grain size dispersion and perfect morphology are crucial here because in the samples with the worse topology the corresponding changes were substantially less. This situation is typically general for optical properties of the NP [21] and a principal role in this case is played by the flattering of the energy bands [22].

4. Conclusions

The complex structural and morphological studies of AuNPs with the regular sizes of 20 nm, 30 nm, 40 nm and 50 nm were performed. Using the hyperfine AFM methods including the surface topology we have classified three types of samples which are different by the sizes. Following the data about the morphology of the AuNP one can conclude that their sizes and shapes are highly

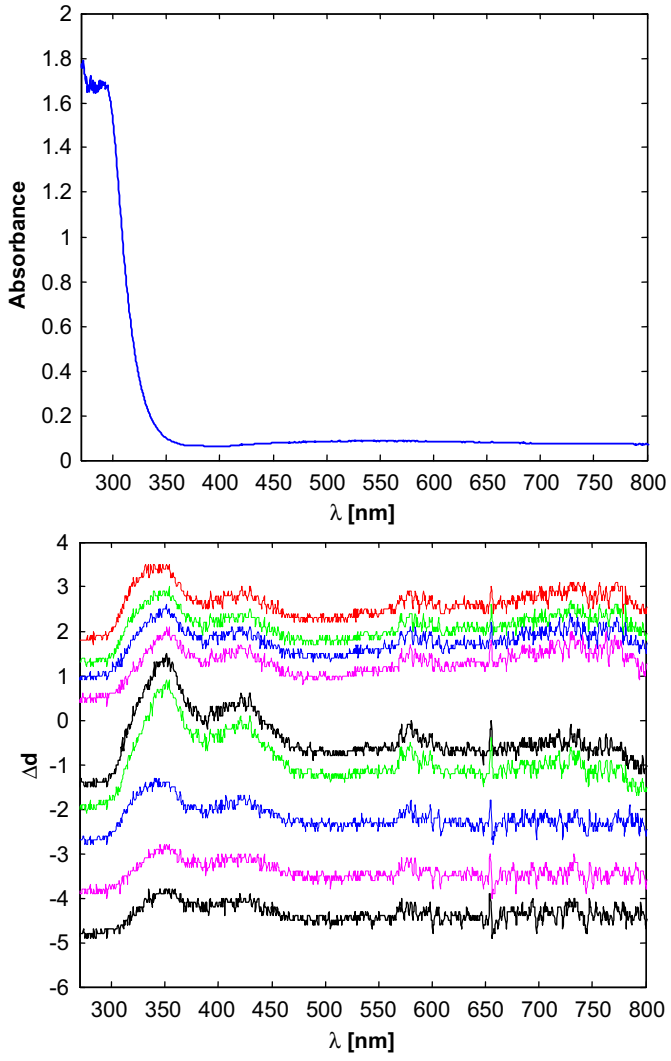

Fig. 5. Typical photoinduced absorption (figure about) and photoinduced absorption (figure below) for the studied AuNP with increasing time of irradiation from 1 min, up to 15 min, during consideration from the up to down. The last two curves correspond to the relaxation times corresponding to 3 min. and 10 min, 532 nm cw laser treatment.

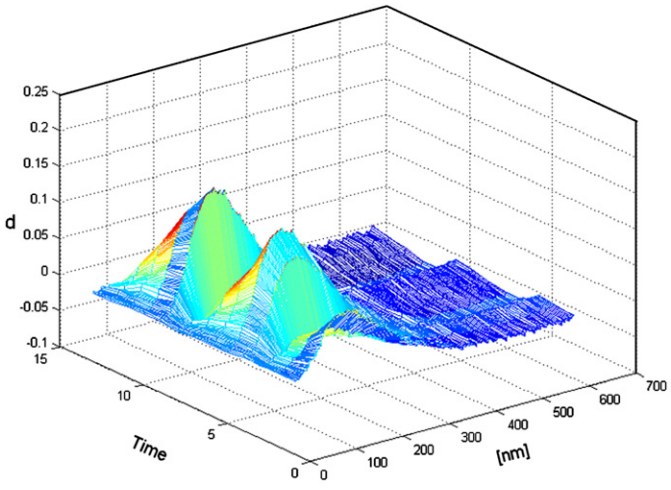

Fig. 6. 3D Photoinduced absorption changes of the studied Au NP.

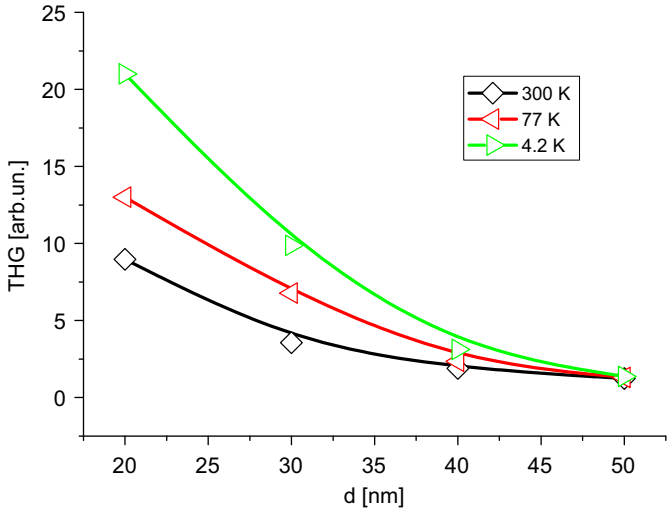

Fig. 7. Dependence of third harmonic generation versus the nanoparticles' sizes at different temperatures.

monodispersed and the inter-particle distances are well defined. The latter is dependent on the sizes of the average AuNP. Such good structural separation of the particular nanoparticles together with their separation from the conducting ITOP substrate is a minimum criterion for their use as materials for perfect interactions with external electromagnetic light and laser coherence particularly. We have found substantial increase of at least two spectral peaks in the photoinduced absorption and we have shown that this process is continued after interruption of the laser dealing. There are three bands observed in the photoinduced absorption spectra of AuNPs/ITO situated at about 350 nm, 430 nm and 580 nm. The first band at about 350 nm is attributed to the interband recombination of the valence d-band electrons with the holes in the conduction sp-band. At the same time we have found a drastic increase of the third harmonic generation during decreasing NP sizes from 50 nm up to 20 nm which may be explained by localized nano-confined effects.

Acknowledgment

For Ali H. Reshak his work was supported from the program RDI of the Czech Republic, the project CENAKVA (no. CZ.1.05/2.1.00/01.0024), the Grant no. 152/2010/Z of the Grant Agency of the University of South Bohemia. School of Material Engineering, Malaysia University of Perlis, P.O. Box 77, d/a Pejabat Pos Besar, 01007 Kangar, Perlis, Malaysia.

References

[1] A. Wei, Plasmonic nanomaterials: enhanced optical properties from metal nanoparticles and their ensembles, in: V. Rotello (Ed.), Nanoparticles: Building Blocks for Nanotechnology, Kluwer Academic/Plenum Publishers, New York, 2004, p. 173.
[2] L. Pasquato, P. Pengo, P. Scrimin, Biological and biomimetic applications of nanoparticles, in: V. Rotello (Ed.), Nanoparticles: Building Blocks for Nanotechnology, Kluwer Academic/Plenum Publishers, New York, 2004, p. 251.
[3] S. Underwood, P. Mulvaney, Langmuir 10 (1994) 3427.
[4] A.C. Templeton, J.J. Pietron, R.W. Murray, P. Mulvaney, Journal of Physical Chemistry. B 104 (2000) 564.
[5] E. Hutter, J.H. Fendler, Advanced Materials 16 (2004) 1685.
[6] W. Knoll, Annual Review of Physical Chemistry 49 (1998) 569.
[7] J. Homola, S.S. Yee, G. Gauglitz, Sensors and Actuators B 54 (1999) 3.
[8] Elka Reiner Dahint, Hatice Trileva, Biosensors and Bioelectronics 22 (2007) 3174–3181.
[9] Ke-Long Zu-Fu Yao, Su-Qin Huang, Xiang-Zhi Liu, Yan-Hua Song, Jun Li, Chemical Engineering Journal 166 (2011) 378.
[10] N.L. Dmitruk, Thin Solid Films 518 (2010) 1737.

[11] Jiajia Deng, Yan Song, Yuan Wang, Junwei Di, Biosensors and Bioelectronics 26 (2010) 615.
[12] Hikaru Tatsuro Endo, Yasunori Takizawa, Yasuko Imai, Takeshi Yanagida, Applied Surface Science 257 (2011) 2560.
[13] Sarah L. Westcott, Steven J. Oldenburg, T. Randall Lee, Naomi J. Halas, Chemical Physics Letters 300 (1999) 651.
[14] Thearith Ung, Luis M. Liz-Marzan, Paul Mulvaney, Gold nanoparticle thin films, Colloids and Surfaces A: Physicochemical and Engineering Aspects 202 (2002) 119.
[15] Ayumi Toyota, Naotoshi Nakashima, Takamasa Sagara, Journal of Electroanalytical Chemistry 565 (2004) 335–342.
[16] Tingyin Ning, Yueliang Zhou, Hong Shen, Heng Lu, Zhihui Sun, Lingzhu Cao, Dongyi Guan, Dongxiang Zhang, Guozhen Yang, Applied Surface Science 254 (2008) 1900.
[17] Weitian Wang, Yanmin Wang, Zhenhong Dai, Yuming Sun, Yuanping Sun, Applied Surface Science 253 (2007) 4673.
[18] V. D'Britto, C.S. Suchand Sandeep, R. Philip, B.L.V. Prasad, Colloids and Surfaces A: Physicochem. Eng. Aspects 352 (2009) 79.
[19] M.A. Aziz, M. Oyama, K. Ozga, A. Wojciechowski, N. Al Zayed, I.V. Kityk, A. Ali Umar, Optics Communications 284 (2011) 245.
[20] Oleg A. Yeshchenko, Igor M. Dmitruk, Alexandr A. Alexeenko, Mykhaylo Yu. Losytskyy, Andriy V. Kotko, Anatoliy O. Pinchuk, Physical Review B 79 (2009) 235438.
[21] V. Rudyk, I. Kityk, V. Kapustianyk, K. Ozga, Ferroelectrics 330 (2006) 19.
[22] I.V. Kityk, A. Kassiba, K.J. Plucinski, J. Berdowski, Physics Letters A V.265A (2000) 403.